Ripple pattern formation on silicon surfaces by low-energy ion-beam erosion: Experiment and theory

B. Ziberi,[1] F. Frost,[1] Th. Höche,[1,2] and B. Rauschenbach[1]
[1]*Leibniz-Institut für Oberflächenmodifizierung e. V., Permoserstrasse 15, D-04318 Leipzig, Germany*
[2]*3D-Micromac AG, Annaberger Str. 240, D-09125 Chemnitz, Germany*
(Received 29 July 2005; revised manuscript received 14 October 2005; published 7 December 2005)

The topography evolution of Si surfaces during low-energy noble-gas ion-beam erosion (ion energy $\leqslant$2000 eV) at room temperature has been studied. Depending on the ion-beam parameters, self-organized ripple patterns evolve on the surface with a wavelength $\lambda < 100$ nm. Ripple patterns were found to occur at near-normal ion incidence angles (5°–30°) with the wave vector oriented parallel to the ion-beam direction. The ordering and homogeneity of these patterns increase with ion fluence, leading to very-well-ordered ripples. The ripple wavelength remains constant with ion fluence. Also, the influence of ion energy on the ripple wavelength is investigated. Additionally it is shown that the mass of the bombarding ion plays a decisive role in the ripple formation process. Ripple patterns evolve for Ar^+, Kr^+, and Xe^+ ions, while no ripples are observed using Ne^+ ions. These results are discussed in the context of continuum theories and by using Monte Carlo simulations.

DOI: 10.1103/PhysRevB.72.235310 PACS number(s): 68.35.−p, 81.65.Cf, 61.82.Fk, 79.20.Rf

I. INTRODUCTION

Low-energy ion-beam sputtering or erosion of solid surfaces is a very effective alternative approach to the generation of self-organized nanostructures. It is well known that under certain conditions, sputtering can roughen the surface, resulting in a pronounced topography, and in some cases well-ordered patterns, like ripples or dots form.[1–5] Such a self-organized process of pattern formation is a simple and inexpensive route for fabricating large-area nanostructured surfaces—e.g., for the deposition of functional thin films. Especially the process of ripple formation has been the subject of many studies since the first observations by Haymann and Navez *et al.*[6] The term ripple formation assumes that in general for off-normal ion-beam erosion of surfaces a quasiperiodic height modulation in a ripple or wavelike structure develops. For the technologically important semiconductor silicon, ripples as well as dot patterns were reported after noble-gas ion-beam erosion.[7–15] According to earlier reports on ripple formation on silicon surfaces under noble-gas ion-beam erosion, two cases can be distinguished: (i) the formation of ripple patterns at relatively high ion energies (typically $E_{ion} \geqslant 20$ keV) at room temperature or below. Under these conditions, the ripples form at ion incidence angles $35° < \alpha_{ion} < 65°$ with respect to the surface normal, with ripple wavelengths above 300 nm.[12–14] Upon ion bombardment, the target surface becomes amorphized. (ii) Ripple patterns are also reported at lower ion energies (e.g., at 750 eV), but at elevated temperatures ($\geqslant$400 °C).[15] In the latter case, ripples form at ion incidence angles near 67° with wavelength >200 nm. Under these erosion conditions the target surface remains crystalline. In general, it can be stated that, independent of ion energy, ripple patterns are observed at ion incidence angles from 40° up to 70° and with ripple wavelengths >100 nm. In contrast, no ripples are reported for low-ion-energy noble-gas sputtering at room temperature, particularly for near-normal ion incidence angles.

In this contribution, recent results on ripple pattern formation on silicon surfaces during low-energy (E_{ion}=500–2000 eV) ion-beam erosion at room temperature are reported. Specifically, the influence of ion incidence angle α_{ion}, ion fluence, and ion energy E_{ion} on the formation, ordering, and size of ripples is investigated. It is observed that ripple patterns form at near-normal ion incidence with wavelength λ well below 100 nm. The wave vector of ripples is aligned parallel to the ion-beam projection on the surface. Experimental results reveal that the wavelength of ripples remains constant with increasing ion fluence, while the ordering increases, leading to ripple patterns with a very high degree of ordering. Additionally, an increase of the ripple wavelength with ion energy is observed in the energy range used in our experiments. Moreover, the influence of different ion species Ne^+, Ar^+, Kr^+, and Xe^+ on ripple formation is investigated. Finally, the consistency of experimental results with existing theoretical models is discussed.

II. EXPERIMENTAL DETAILS

Samples used in this work were commercially available epi-polished Si(100) substrates (p type and 0.01–0.02 Ω cm), with a root-mean-square (rms) roughness of ~0.2 nm. The samples were mounted on a water-cooled substrate holder. The angle of the ion-beam incidence, α_{ion}, can be varied between 0° and 90° with respect to the surface normal. For ion-beam erosion experiments, a homebuilt Kaufman-type broad beam ion source equipped with a two-grid ion optical system (beam diameter 200 mm) was employed. The operating conditions of the ion source were optimized such that well-defined ion energy distributions were attained.[16,17] The ion current density j_{ion} was kept constant at about 300 μA cm^{-2} corresponding to an ion flux of 1.87×10^{15} cm^{-2} s^{-1}. The ion fluence was varied from 1.12×10^{17} cm^{-2} up to 1.35×10^{19} cm^{-2}, corresponding to an erosion time of 60 s up to 7200 s, respectively.

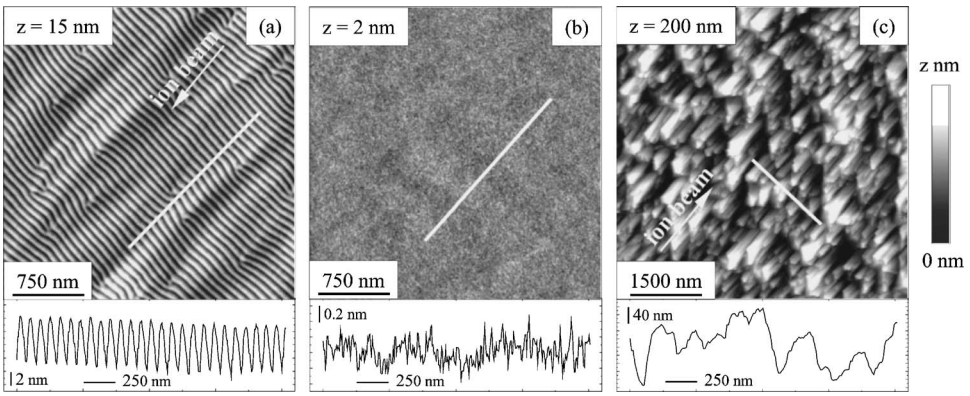

FIG. 1. AFM images of Xe^+ ion-beam-eroded Si surfaces (ion fluence of 6.7×10^{18} cm^{-2}, E_{ion}=2000 eV) at different ion incidence angles: (a) 5°, (b) 45°, and (c) 75°. The image sizes are 3 μm$\times$3 μm (a), (b) and 6 μm$\times$6 μm (c). Note the deviating (vertical) z scales. The cross-section profiles show the height modulations along the white lines (2 μm in length) indicated in the AFM images.

The surface topography was analyzed by scanning-force microscopy (AFM). Measurements were performed in air using silicon cantilevers with a nominal tip radius less than 10 nm. In order to study the lateral ordering and the characteristic wavelength of ripples, the Fourier transformation (FFT) of the height profile was calculated. From the Fourier transformation the one-dimensional power spectral density (PSD) function was obtained by angular averaging.[18] High-resolution transmission electron microscopy (HRTEM) was performed with a 400-keV microscope possessing a point resolution of 0.155 nm to study the shape and structure of ripples in a cross section.

III. RESULTS

A representative example of surface evolution by ion-beam erosion with varying incidence angle (α_{ion}) is given in Fig. 1. The target was bombarded with 2000-eV Xe^+ ions at a total ion fluence of 6.7×10^{18} cm^{-2}, corresponding to 3600 s erosion time. Starting at normal incidence, dot structures develop on the surface (not shown here), similar to those reported by Gago *et al.*[8] By changing the incidence angle to 5°, ordered ripple patterns evolve on the surface [Fig. 1(a)]. The wave vector of ripples (with wavelength 77 nm) is aligned parallel to the projection of the ion beam. Pattern formation is observed for ion incidence angle up to 30°. By further increasing the ion incidence angle to 45° no ripple patterns form on the surface; i.e., the surface remains smooth even after long-time sputtering [Fig. 1(b)]. At grazing incidence (75°) the surface roughens again and certain features (pillars) develop on the surface. These features form in the direction of the incoming ion beam, and their size increases with erosion time [Fig. 1(c)]. A similar incidence angle dependence is observed for Ar^+ or Kr^+ ions. Surprisingly, no ripple patterns evolve on the Si surface when using Ne^+ ions. This indicates that, especially in the low-energy range used in these experiments, the mass of the impinging ions plays a decisive role in the ripple formation process; i.e., a minimum mass of the projectile is required to initiate ripple formation. This is different compared to results of Carter *et al.*[19] who reported about the formation of irregular wavelike structures on Si, however by using 20-keV Ne^+ ions, at lower temperatures (120 K).

The evolution of the surface topography with ion incidence angle for erosion with Ar^+, Kr^+, and Xe^+ ions is quantitatively summarized in Fig. 2 where the dependence of the root-mean-square (rms) roughness on α_{ion} is plotted. The rms roughness can be taken as a measure for the height fluctuation on the surface—i.e., the ripple amplitude. Generally, three different regions can be distinguished. In the first region (I) ranging up to 30° ion incidence ripple patterns develop on the surface. By increasing the ion incidence angle the amplitude of the ripples decreases. Also the ripple wavelength decreases with ion incidence angle. For ion incidence angles between 35° and 60° (region II), the surface remains smooth, independent of the ion energy and ion species used for the experiments. It is worth mentioning that these ion-beam conditions can be used for direct ion-beam smoothing of surfaces.[20,21] In region III (between approximately 65° and 85°), the surface roughens again and columnar (pillar) structures evolve on the surface with much larger amplitudes than ripples in region I.

In the following the focus will be on ripple formation at near-normal ion incidence angle. The influence of ion fluence and ion energy on the ordering and size of ripples will be

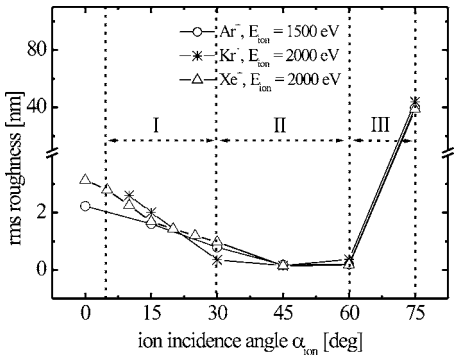

FIG. 2. Evolution of surface roughness with ion incidence angle for different ion species (Ar^+, Kr^+, and Xe^+). The ion fluence was fixed to 6.7×10^{18} cm^{-2} (erosion time 3600 s). I, II, and III are the three regions where different topographies evolve on the target surface (see explanation in text).

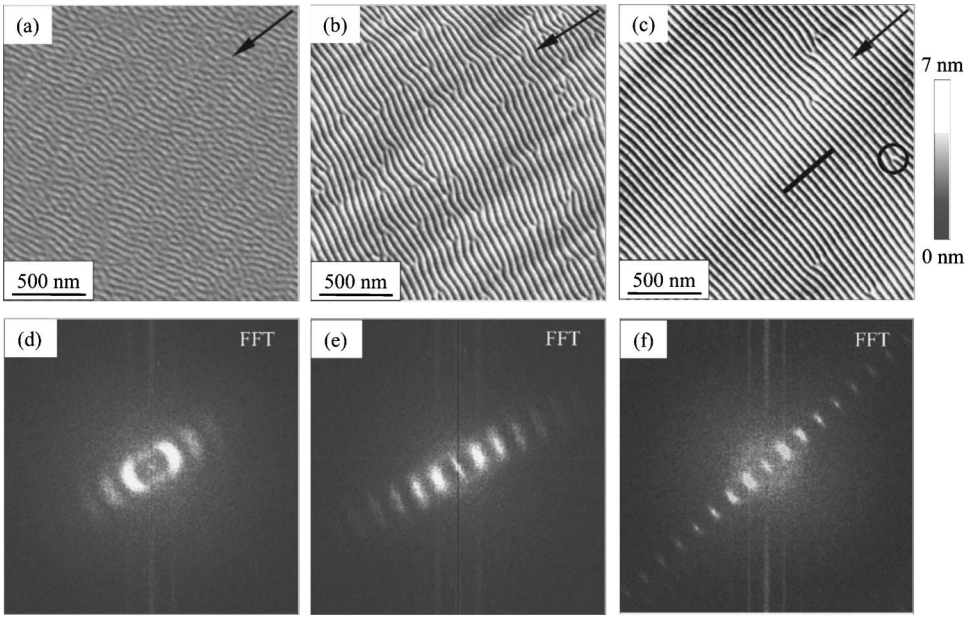

FIG. 3. Self-organized Si ripple patterns produced by Kr^+ ion-beam erosion at $E_{ion}=1200$ eV, $a_{ion}=15°$, for different ion fluences: (a) 3.36×10^{17} cm^{-2}, (b) 2.24×10^{18} cm^{-2}, and (c) 1.34×10^{19} cm^{-2}. (a)–(c) 2 μm$\times$2 μm AFM images (the arrows give the ion-beam direction). (d)–(f) Corresponding Fourier spectrum (image range ±127.5 μm^{-1}). The circle in (c) shows the defects on the AFM image. The bar in (c) corresponds to a cross-section profile given in Fig. 7(b).

discussed in detail. Examples of ripple evolution with increasing ion fluence during Kr^+ ion-beam erosion of Si surfaces ($\alpha_{ion}=15°$ and $E_{ion}=1200$ eV) are presented in Fig. 3. The experimental observations reveal that ripples start to form immediately after the beginning of the bombardment. The AFM image in Fig. 3(a) shows the ripple pattern after bombarding with an ion fluence of 3.3×10^{17} cm^{-2}. The corresponding Fourier image [Fig. 3(d)] reveals that the wave vector of the ripples runs parallel to the projection of the ion beam onto the surface. The position of the first peak specifies the characteristic wave vector of the ripples—i.e., the ripple wavelength. The radial width of the peak shows how ordered the ripples are; i.e., the smaller the width of the peak, the more ordered are the ripples. Moreover, the angular width of the Fourier peak (which gives the angular distribution of the ripples) decreases with erosion time. That means the homogeneity and ordering (alignment) of ripples becomes improved. The appearance of higher-order peaks is an additional sign of the improved ripple ordering. As sputtering proceeds [Fig. 3(b), after sputtering with an ion fluence of 2.24×10^{17} cm^{-2}], the ordering and homogeneity of the ripples increase [Fig. 3(e)] and the number of defects [marked with a circle in Fig. 3(c)] decreases. For prolonged sputtering (ion fluence of 1.35×10^{19} cm^{-2}), the ripples are almost perfectly aligned, as can be seen in the AFM image of Fig. 3(c). There are approximately two defects per 1 μm^2. In the corresponding FFT image [Fig. 3(f)], the number of higher-order peaks increases while the radial as well as the angular width of the peak decreases. Additionally to the dominating ripple structures, also corrugations with the wave vector perpendicular to the ion-beam direction form on the surface. These corrugations coarsen with time until they saturate similar to short-wavelength ripples. Because of the fluctuations on the lateral size, it is difficult to determine their wavelength. The amplitude of corrugations is very small compared to short-wavelength ripples, even after large ion fluences (up to 4×10^{19} cm^{-2}). On the contrary, Brown *et al.* reported about a transition of ripples with ion fluence from the parallel mode to the perpendicular mode.[22] However, their experiments were performed at high temperatures.

In order to quantify the evolution of the ripple pattern with ion fluence, and in particular the wavelength of ripples and their ordering, the angularly averaged PSD functions are calculated from the Fourier images [Fig. 4]. For comparison, the PSD function of a noneroded surface is given in Fig.

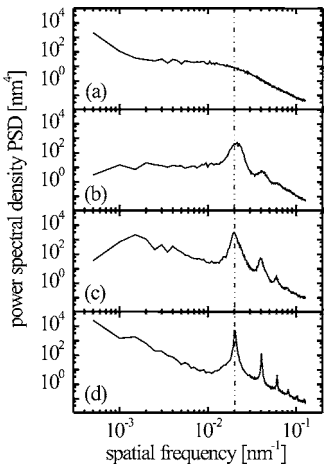

FIG. 4. (b)–(d) Angular-averaged PSD functions obtained from Fourier images in Figs. 3(d)–3(f). For comparison the PSD function of an untreated (not eroded) surface is given (a). The peak giving the characteristic ripple wavelength is observed at the same position-independent of ion fluence. The number of multiple peaks increases with ion fluence.

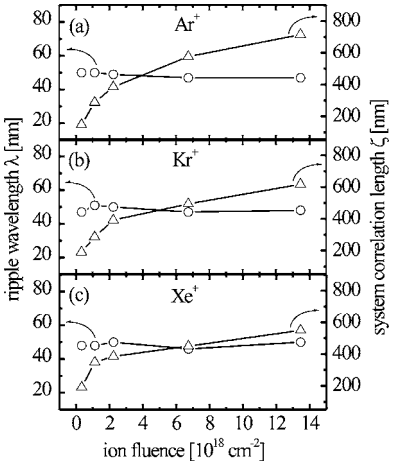

FIG. 5. Evolution of ripple wavelength and system correlation length with ion fluence for $E_{ion}=1200$ eV, $\alpha_{ion}=15°$. (a) Ar^+, (b) Kr^+, and (c) Xe^+.

4(a). From the position of the peak and its width the characteristic wavelength and the lateral ordering of ripples can be quantitatively derived. The position of the first peak in the PSD functions gives an average ripple wavelength $\lambda \sim 50$ nm. Further, the position of the first peak is not shifting with ion fluence; i.e., the wavelength of ripples remains constant (in fact, the wavelength was constant even after sputtering with an ion fluence of 4×10^{19} cm^{-2}, not shown here). These observations are quantitatively summarized in Fig. 5, where the evolution of the ripple wavelength λ and the system correlation length ζ with ion fluence, for Ar^+, Kr^+, and Xe^+ ion-beam erosion is given. The system correlation length ζ is a measure for the lateral ordering of structures on the surface, and it gives the length scale up to which positional correlation is present—i.e., the average domain size.[18,23] It is calculated from the full width at half maximum (FWHM) of the first-order PSD peak and is inversely proportional to the FWHM. In Fig. 5, a similar behavior is observed for Ar^+, Kr^+, and Xe^+ ions. While no variation of the ripple wavelength with ion fluence is observed, the system correlation length ζ increases with ion fluence. At the beginning (up to an ion fluence of 2×10^{18} cm^{-2}) there is a steeper increase than for larger ion fluences. For larger fluences, the domain size extends up to 720 nm. These results are different from earlier reports on Si, where a variation of ripple wavelength with ion fluence was observed.[9,12]

Further, the evolution of the rms roughness, as a measure for the ripple amplitude, with ion fluence is studied. Figure 6 shows the rms roughness data deduced from AFM images for Ar^+, Kr^+, and Xe^+ ions. For small ion fluences of sputtering, up to 5.6×10^{17} cm^{-2}, the roughness seems to grow exponentially (see the dotted line in Fig. 6). For an ion fluence of approximately 1×10^{18} cm^{-2}, the roughness—i.e., the ripple amplitude—saturates and it remains constant upon further sputtering. The results in Fig. 6 prove that the evolution of ripple amplitude with ion fluence is similar for different ion species including Ar^+, Kr^+, and Xe^+. The results are in agreement with earlier reports on the roughness evolution with ion fluence on Si.[15]

In order to study the shape and structure of ripples, high-resolution transmission electron microscopy imaging of the

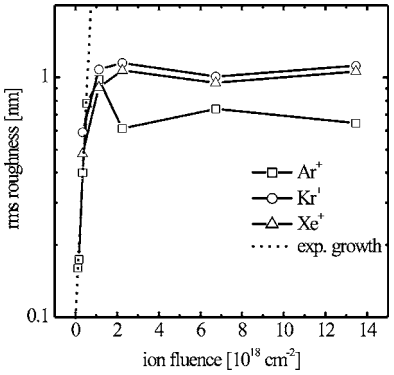

FIG. 6. Evolution of the rms surface roughness with ion fluence for Ar^+, Kr^+, and Xe^+ ions ($E_{ion}=1200$ eV, $\alpha_{ion}=15°$). The dotted line corresponds to an exponential growth the of the surface roughness for the initial stage of sputtering.

sample shown in Fig. 3(c) was performed [Fig. 7(a)]. The HRTEM image reveals an amorphous layer covering the Si surface, with a thickness of about 6 nm. This amorphization is expected because the total ion fluence used in the experiments is several orders of magnitude higher than the amorphization threshold amounting to $\sim10^{15}$ ions cm^{-2}, as reported during 2-keV Xe^+ bombardment on Si.[24] Beneath the amorphous layer, the surface is single crystalline. In the HRTEM image, there is evidence for a strong correlation on the shape of ripples in *a*-Si and *c*-Si layers. Furthermore, ripples possess a slight asymmetry; i.e., the side facing the ion beam is slightly less steep than the other side. This observation correlates with the cross-section profile taken from the corresponding AFM image [Fig. 7(b)], where also a certain asymmetry of ripples is observed. The inclination angle of the site facing the ion beam is ~2 times smaller than the other side.

Eventually, the evolution of the ripple wavelength with ion energy E_{ion} was studied [Fig. 8]. The target surface was irradiated with Ar^+, Kr^+, and Xe^+ ions at $\alpha_{ion}=15°$ and a total fluence of 6.7×10^{18} cm^{-2}. The graph shows that the ripple wavelength λ increases with ion energy (from 500 to 2000 eV) from 40 to 70 nm. Also in Fig. 8 the ratio of the system correlation length normalized to the mean wavelength of ripples is plotted. The ratio gives the number of nearest-neighbor distances of ordered ripples. The ratio implies that ripples with the best ordering are obtained at an ion energy of 1200 eV. The dependency $\lambda(E_{ion})$ corresponds with previ-

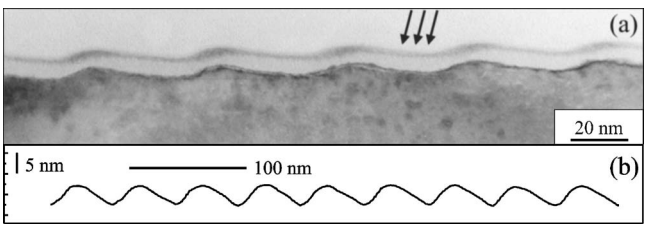

FIG. 7. (a) Cross-sectional HRTEM image of ripple patterns. The amorphous covering layer has a thickness of 6 nm. The arrows give the direction of the ion beam. (b) Cross-section profile of ripples from the AFM image in Fig. 3(c) confirming the ripple asymmetry.

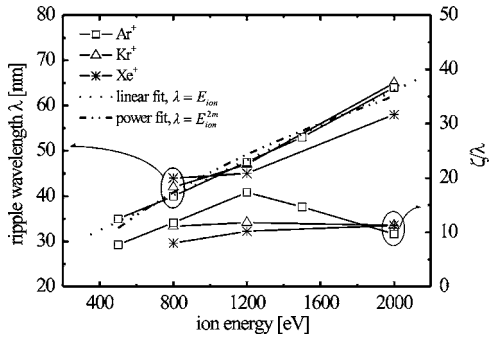

FIG. 8. Evolving ripple wavelength and system correlation length (normalized to the ripple wavelength) with ion energy for different ion species ($\alpha_{ion}=15°$, total ion fluence of 6.7×10^{18} cm^{-2}). Also the linear fit and power fit (with a slope $m=0.22$) of data in the case of Ar^+ ions are given.

ous reports on Si and graphite, where also an increase in the size of ripples with ion energy is observed.[25,26] In order to study the evolution of the wavelength λ with ion energy E_{ion} (see Sec. IV) a linear ($\lambda \propto E_{ion}$) and power ($\lambda \propto E_{ion}^{2m}$) fit of the data for the case of Ar^+ was performed. The power-law fit gives an exponent $m=0.22$. From the fitted curves and the energy range used, it is difficult to distinguish between a linear and a power dependence of the wavelength on ion energy.

IV. DISCUSSION

Theoretically the process of ripple formation is described by the linear Bradley-Harper (BH) model.[27] According to this model, the formation of ripple patterns is due to the instability caused by the competition between curvature-dependent sputtering that roughens the surface and different surface relaxation mechanisms (e.g., surface diffusion). Following the BH model, the surface height evolution $h(r,t)$ can be described by

$$\partial_t h = \nu_x \partial_x^2 h + \nu_y \partial_y^2 h - D\nabla^4 h. \tag{1}$$

For simplicity the zeroth-and first-order terms (which do not influence the process of pattern formation itself) are omitted. In Eq. (1), $\nu_{x,y}$ are the effective surface tension coefficients generated by the erosion process, dependent on the ion incidence angle and on the local surface curvature. D is the relaxation coefficient due to the (thermally activated) surface diffusion. Depending on the value of the parameters ν_x and ν_y the wave vector of ripples is oriented parallel or perpendicular to the projection of the ion beam on the surface. From Eq. (1) at off-normal ion incidence BH derived a relation for the ripple wavelength $\lambda=2\pi(2D/|\nu|)^{1/2}$, where $|\nu|$ is the largest in absolute value of the ν_x and ν_y coefficients. According to the BH model the coefficient ν (for a given ion incidence angle) is calculated from the distribution of the deposited energy density F_D on the surface from the incoming ions. F_D is deduced by using Sigmunds linear cascade theory of sputtering of amorphous targets, and it has a Gaussian form[28,29]

$$F_D(x,y,z) = \frac{E_{ion}}{(2\pi)^{3/2}\alpha\beta^2}\exp\left[-\frac{(z-h_0-a)^2}{2\alpha^2}-\frac{x^2+y^2}{2\beta^2}\right]. \tag{2}$$

It gives the average energy deposited at a certain point in the target by an ion which travels along the direction of the incoming ions. Here a is the mean penetration depth and α and β are the width of the distribution parallel and perpendicular to the incoming ion beam, respectively. The values of the parameters a, α, and β depend on the kinematics between the projectile and target atoms. Other theories based on the BH model include additional terms to account for nonlinear effects and the stochastic nature of ion arrival at the surface.[30–32] These theories predict the evolution of ripple patterns at intermediate ion fluences and an amplitude saturation at higher fluences. For prolonged sputtering, the surface topography is characterized by kinetic roughening or by the appearance of a new type of ripples.[32,33] Recently Castro *et al.* proposed a new continuum model that can account for the amplitude saturation for prolonged sputtering.[34] The evolution of the surface roughness with ion fluence coincides very well with our experimental results. However, they also predict a coarsening of the structure size with ion fluence at the initial stage of sputtering. This coarsening is not observed in our experimental studies (Fig. 5).

Under the experimental conditions given, thermally activated surface diffusion coefficients as proposed by BH can be ruled out as a dominant relaxation mechanism. Otherwise, one would expect a decrease of the ripple wavelength with ion energy. This is not, however, observed experimentally (Fig. 8). Also, for experiments performed at room temperature, no time-dependent surface relaxation is observed after the ion beam is turned off. Makeev and Barabasi[35] introduced a mechanism called ion-induced effective surface diffusion (ESD) that can lead to preferential erosion and mimics a surface diffusion process, but without mass transport along the surface. This mechanism is temperature independent and can be determined by the sputter parameters and the distribution of the deposited energy.[32,35] If ion-induced ESD is the dominating mechanism, then the ripple wavelength depends linearly on the mean penetration depth $a\lambda \propto a \propto E_{ion}^{2m}$, where m characterizes the interatomic potential employed to describe the interaction between the ion and target atoms.[29,36,37] For the energy range used in our experiments m has values <0.5.

In our experimental studies, the formation of ripple patterns at near-normal ion incidence, with a wave vector oriented parallel to the ion-beam direction, is observed. Although an alignment of features parallel to the ion-beam direction is found for large incidence angles [Fig. 1(c)], no ripples comparable to those at near-normal incidence and with the wave vector oriented perpendicular to the incoming ion beam appear. It is worth mentioning that all experimental studies reported so far give an angle of incidence above 35° for the formation of ripples.[4,38] Further, the experimental results show that ripple patterns are stable upon prolonged sputtering and there is no crossover to kinetic roughening or to some new types of ripples, as predicted by theory.[33]

Assuming that ion-induced ESD is the dominating relaxation process, using the expressions given by Makeev, Cu-

TABLE I. Calculated wavelength (λ) of ripples for different ion species. Parameters a, α, and β were calculated using the SRIM code (Ref. 36). Coefficients ν_x and D_x were calculated using the relations given by Makeev, Cuerno, and Barabasi (Ref. 31).

Ion species	a (nm)	α (nm)	β (nm)	ν_x (nm)	D_x (nm^3)	λ (nm)
Ar^+	2.5	2	1.6	−0.459	0.332	7.54
Kr^+	2.2	1.6	1.1	−0.29	0.107	5.4
Xe^+	2.1	1.4	0.8	−0.18	0.037	4.02

erno, and Barabasi for D_x and ν_x, it is possible to calculate the ripple wavelength.[32] For a given incidence angle, the normalized coefficients D_x and ν_x depend on the parameters a, α, and β (for details, see Ref. 31). In Table I, the parameters a, α, and β, calculated using the simulation code SRIM (Ref. 39) and the approach of Bolse[40] for normal ion incidence, are given. The coefficients D_x and ν_x were calculated for $E_{ion}=1200$ eV and $\alpha_{ion}=15°$.

From the calculated wavelength values (λ) given in Table I, a difference up to 40% between the wavelengths for Ar^+ and Xe^+ is observed. But from our experimental studies, no dependence of the ripple wavelength is observed for Ar^+, Kr^+, and Xe^+ ions (Fig. 5). Also, the calculated values are an order of magnitude smaller than the experimental one. An indication that the ESD term alone cannot account for the observed wavelength of ripples and other relaxation terms should be considered (e.g., viscous flow). Similar results were observed by Umbach *et al.*[41] From the above considerations, a disagreement between calculated values and experimental results is evident.

In Fig. 9(a) the calculated values for the mean depth a for different ion species and different ion energies for normal incidence using the SRIM code are plotted. A power-law fit $a(E) \propto E_{ion}^{2m}$ of the data for Ar^+ is performed, giving an exponent $m=0.31$. This is in reasonable agreement with the experimental exponent ($m=0.21$) if the power fit is considered. But to address this point in detail, it is mandatory to extend the ion energy range.

Additionally, experiments showed that there is no structure formation when Ne^+ ions are used to bombard the silicon surface. There are two possible explanations for this observation

(i) With increasing ion mass, the energy deposition in the near-surface region increases, leading to an enhancement of the curvature-dependent sputtering. In Fig. 9(b) the depth profile of the deposited energy F_D for Ne^+ and Ar^+ ions at 2000 eV is plotted. The lines correspond to fits using Eq. (2). It is known from the theory and experiments that the main contribution to the sputter yield comes from the atoms ejected from the uppermost surface layers.[24] The ejected atoms originate mainly from the recoils created in the near-surface region. From Fig. 9(b) the mean penetration depth and the width of distribution of the deposited energy for Ar^+ ions is smaller than for Ne^+. This means, in the case of Ar^+, that more energy is deposited in the near-surface region than for Ne^+; i.e., more recoils are created in the near-surface region in the case of Ar^+.

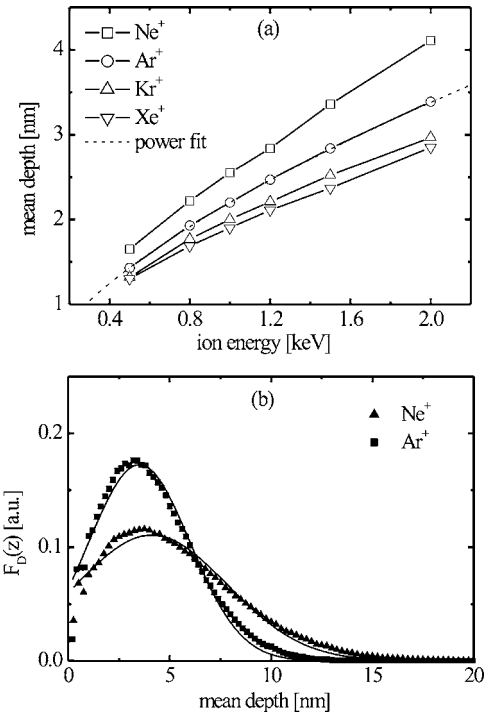

FIG. 9. (a) Results from the SRIM code simulations for the mean depth a of the deposited energy for different energies and different ion species. A power-law fit of data for Ar^+ is performed giving a slope $m=0.31$. (b) Depth distribution of the deposited energy as simulated with SRIM for Ne^+ and Ar^+ ions with 2000 eV and for normal incidence. The solid lines represent a fit using Eq. (2).

(ii) In addition to the energy deposition also highly energetic sputtered target atoms as well as backscattered projectile ions become more important for decreasing ion mass. This was confirmed by SRIM (Ref. 37) calculations, revealing that for lighter projectile ions the number of highly energetic atoms sputtered at oblique incidence (0° up to 15° with respect to the surface plane) is higher when Ne^+ ions are used compared to Ar^+ and Kr^+ ions. These sputtered particles contribute to additional sputtering of peaks compared to valleys, hence prohibiting the evolution of ripples and leading to smooth surfaces.[42]

V. CONCLUSIONS

In conclusion, a detailed study of the evolution of the surface topography after low-energy noble-gas ion-beam erosion was performed. It was shown that ripple patterns evolve on silicon surfaces at near-normal ion incidence (5°–30°) for Ar^+, Kr^+, and Xe^+ ions. The ordering of these structures increases with ion fluence, leading to remarkably well-ordered ripples. In contrast, the wavelength of the ripples remains constant with ion fluence. It was also shown that the ripple amplitude increases rapidly for small ion fluences and it passes over into a steady state with increasing ion fluence. Experimental results reveal no disappearance of ripples for prolonged sputtering or the appearance of new types of ripples, as expected from the theory. The wavelength of ripples increases with ion energy (ranging from 35 nm up to

65 nm), and at 1200 eV ripples seems to have the highest ordering. Our experimental results reveal no difference in the morphological evolution of ripples when using Ar^+, Kr^+, or Xe^+ ions. This wavelength evolution it seems inconsistent with the theoretical calculations when ion-enhanced surface diffusion is considered as the main relaxation mechanism, where a decrease of the ripple wavelength with ion mass is expected. Also possible explanations are given about the absence of ripple formation using Ne^+ ions. The Monte Carlo simulations reveal that in the case of Ar^+ more energy is distributed in the near-surface region than for Ne^+ ions. Those creating more recoils in the near-surface region in the case of Ar^+ contribute mainly to the ejection of the surface atoms.

ACKNOWLEDGMENTS

The authors would like to thank Professor U. Gösele (Max-Planck-Institut für Mikrostrukturphysik Halle, Germany) for enabling the TEM measurements. This work is supported by Deutsche Forschungsgemeinschaft.

[1] S. Rusponi, C. Boragno, and U. Valbusa, Phys. Rev. Lett. **78**, 2795 (1997).
[2] S. Facsko, T. Dekorsy, C. Koerdt, C. Trappe, H. Kurz, A. Vogt, and H. L. Hartnagel, Science **285**, 1551 (1999).
[3] F. Frost, A. Schindler, and F. Bigl, Phys. Rev. Lett. **85**, 4116 (2000).
[4] U. Valbusa, C. Boragno, and F. Buatier de Mongeot, J. Phys.: Condens. Matter **14**, 8153 (2002).
[5] F. Frost, B. Ziberi, T. Höche, and B. Rauschenbach, Nucl. Instrum. Methods Phys. Res. B **216**, 9 (2004).
[6] P. Haymann, Acad. Sci., Paris, C. R. **248**, 2472 (1959); M. Navez, C. Sella, and D. Chaperot, *ibid.* **254**, 240 (1962).
[7] G. Carter, J. Phys. D **34**, R1 (2001).
[8] R. Gago, L. Vázquez, R. Cuerno, M. Varela, C. Ballesteros, and J. M. Albella, Appl. Phys. Lett. **78**, 3316 (2001).
[9] S. Habenicht, K. P. Lieb, J. Koch, and A. D. Wieck, Phys. Rev. B **65**, 115327 (2002).
[10] B. Ziberi, F. Frost, T. Höche, and B. Rauschenbach in Kinetics-Driven Nanopatterning on Surfaces, edited by Eric Chason, George H. Gilmer, Hanchen Huang, and Enge Wang Mater. Res. Soc. Symp. Proc. No. 849 (Materiels Research Society, Warrendale, PA, 2005).
[11] B. Ziberi, F. Frost, and B. Rauschenbach, Appl. Phys. Lett. **87**, 1 (2005).
[12] G. Carter and V. Vishnyakov, Phys. Rev. B **54**, 17647 (1996).
[13] T. K. Chini, M. K. Sanyal, and S. R. Bhattacharyya, Phys. Rev. B **66**, 153404 (2002).
[14] S. Hazra, T. K. Chini, M. K. Sanyal, J. Grenzer, and U. Pietsch, Phys. Rev. B **70**, 121307 (2004).
[15] J. Erlebacher, M. J. Aziz, E. Chason, M. B. Sinclair, and J. A. Floro, Phys. Rev. Lett. **82**, 2330 (1999).
[16] M. Zeuner, J. Meichsner, H. Neumann, F. Scholze, and F. Bigl, J. Appl. Phys. **80**, 611 (1996).
[17] M. Tartz, E. Hartmann, F. Scholze, and H. Neumann, Rev. Sci. Instrum. **69**, 1147 (1998).
[18] Y.-P. Zhao, G.-C. Wang, and T.-M. Lu, *Characterization of Amorphous and Crystalline Rough Surfaces: Principles and Applications* (Academic Press, San Diego, 2001).
[19] G. Carter, V. Vishnyakov, Yu. V. Martynenko, and M. J. Nobes, J. Appl. Phys. **78**, 3559 (1995).
[20] M. Wißing, M. Batzill, and K. J. Snowdon, Nanotechnology **8**, 40 (1997).
[21] F. Frost, R. Fechner, D. Flamm, B. Ziberi, W. Frank, and A. Schindler, Appl. Phys. A: Mater. Sci. Process. **78**, 651 (2004).
[22] A.-D. Brown, J. Erlebacher, W. L. Chan, and E. Chason, Phys. Rev. Lett. **95**, 056101 (2005).
[23] M. Schmidbauer, *X-Ray Diffuse Scattering from Self-Organized Mesoscopic Semiconductor Structures* (Springer, Berlin, 2004).
[24] H. Gnaser, *Low-Energy Ion Irradiation of Solid Surfaces* (Springer, Berlin, 1999).
[25] G. Carter, V. Vishnyakov, and M. J. Nobes, Nucl. Instrum. Methods Phys. Res. B **115**, 440 (1996).
[26] S. Habenicht, Phys. Rev. B **63**, 125419 (2001).
[27] R. M. Bradley, and J. M. E. Harper, J. Vac. Sci. Technol. A **6**, 2390 (1988).
[28] P. Sigmund, Phys. Rev. **184**, 383 (1969).
[29] P. Sigmund, J. Mater. Sci. **8**, 1545 (1973).
[30] R. Cuerno and A.-L. Barabási, Phys. Rev. Lett. **74**, 4746 (1995).
[31] M. Rost and J. Krug, Phys. Rev. Lett. **75**, 3894 (1995).
[32] M. A. Makeev, R. Cuerno, and A. L. Barabasi, Nucl. Instrum. Methods Phys. Res. B **197**, 185 (2002).
[33] S. Park, B. Kahng, H. Jeong, and A.-L. Barabasi, Phys. Rev. Lett. **83**, 3486 (1999).
[34] M. Castro, R. Cuerno, L. Vàzquez, and R. Gago, Phys. Rev. Lett. **94**, 016102 (2005).
[35] M. A. Makeev and A.-L. Barabási, Appl. Phys. Lett. **71**, 2800 (1997).
[36] *Sputtering by Particle Bombardment*, edited by R. Behrisch (Springer-Verlag, Heidelberg, 1983), Vols. I and II.
[37] The proportionality between the mean depth and the ion energy is given by Sigmunds theory of sputtering (see Ref. 28).
[38] G. Carter, Phys. Rev. B **59**, 1669 (1999).
[39] J. F. Ziegler, J. P. Biersack, and U. Littmark, *The Stopping and Range of Ions in Solids* (Pergamon, New York, 1985).
[40] W. Bolse, Mater. Sci. Eng., R. **12**, 53 (1994).
[41] Similar observations are reported by C. C. Umbach, R. L. Headrick, and K.-C. Chang, Phys. Rev. Lett. **87**, 246104 (2001).
[42] F. Frost, B. Ziberi, and B. Rauschenbach (unpublished).